nature neuroscience

# Orientation tuning of cytochrome oxidase patches in macaque primary visual cortex

John R Economides[1,4], Lawrence C Sincich[2,4], Daniel L Adams[1,3] & Jonathan C Horton[1]

**The abundant concentration of cytochrome oxidase in patches or blobs of primate striate cortex has never been explained. Patches are thought to contain unoriented, color-opponent neurons. Lacking orientation selectivity, these cells might endow patches with high metabolic activity because they respond to all contours in visual scenes. To test this idea, we measured orientation tuning in layer 2/3 of macaque cortical area V1 using acutely implanted 100-electrode arrays. Each electrode recording site was identified and assigned to the patch or interpatch compartment. The mean orientation bandwidth of cells was 28.4° in patches and 25.8° in interpatches. Neurons in patches were indeed less orientation selective, but the difference was subtle, indicating that the processing of form and color is not strictly segregated in V1. The most conspicuous finding was that patch cells had a 49% greater overall firing rate. This global difference in neuronal responsiveness, rather than an absence of orientation tuning, may account for the rich mitochondrial enzyme activity that defines patches.**



In people with lesions of the fusiform gyrus the perception of color is abolished, although the ability to detect form remains intact[1]. It is unclear where the pathways that serve color and form begin to diverge in the visual system. In the retina, most ganglion cells do double duty, conveying information about both form and color. Once their signals have been filtered by the lateral geniculate nucleus and reach the primary visual cortex (striate cortex, V1), are the sensations of form and color mediated by separate populations of cells?

There are two compartments in the primary visual cortex, distinguished by the distribution of a mitochondrial enzyme, cytochrome oxidase. Histochemical staining for the enzyme reveals a regular pattern of dark patches ('blobs', 'puffs'), surrounded by paler tissue[2,3]. Tangential microelectrode penetrations through striate cortex have shown that neurons in blobs do not show orientation selectivity, whereas cells between blobs are highly orientation selective. In addition, blob cells have color-opponent receptive field properties. These two key findings—lack of orientation selectivity and color opponency—have led to the view that in V1 "a system involved in the processing of color information, especially color-spatial interactions, runs parallel to and separate from the orientation-specific system"[4]. This functional segregation could explain the dissociation of color and form perception in the visual system, but it has hinged on the considerable challenge of correlating the receptive field properties of individual cells with the location of cytochrome oxidase patches in striate cortex[5].

Recently, 100-electrode arrays have become available for recording single cells in the cerebral cortex[6–9]. These devices permit a quantitative assessment of any receptive field parameter for scores of cells simultaneously, eliminating the one-cell-at-a-time bottleneck of the single microelectrode. They also eliminate the need to extrapolate between lesions along a microelectrode trajectory to infer the position of recording sites. Each electrode in the array leaves a small defect, allowing one literally to pinpoint each V1 recording site with respect to the cortical layers and the cytochrome oxidase patches. Although designed for chronic implantation in alert, behaving animals, multielectrode arrays can be used for acute recordings[6]. Here, we have used them to examine the orientation specificity of cells in macaque striate cortex, comparing the tuning of cells in cytochrome oxidase patches versus interpatches.

## RESULTS

### Alignment of electrodes with cytochrome oxidase patches

Electrode arrays were implanted in opercular V1, representing eccentricities between 2° and 8° (**Supplementary Fig. 1**). When most of the electrodes penetrated only the superficial cortical layers, the array footprint was not immediately obvious in histological sections (**Fig. 1a**). Nonetheless, all 100 holes could be located by searching carefully in tangential sections through layer 2/3 processed for cytochrome oxidase activity (**Fig. 1b**). It was vital to be sure that each hole was truly from an electrode shaft, not a blood vessel. Occasional blood clots, caused by hemorrhage along the electrode shafts, and small clumps of red blood cells were helpful for identifying electrode holes. In addition, electrode holes could be distinguished from blood vessels by noting their grid-like spacing, absence of bifurcations, lack of endothelium and tendency to end in the same cortical layer as adjacent holes.

Our goal was to record from cells in layer 2/3, where patches have maximum contrast, to compare our results directly to those reported previously[4]. For this reason, it was crucial to figure out the layer in which each electrode tip ended. This was accomplished by systematically following each electrode hole from the pial surface, section by section through the cortex, until it disappeared (**Fig. 2**). Sometimes the pneumatic device used to insert the array propelled

[1]Beckman Vision Center, University of California, San Francisco, San Francisco, California, USA. [2]Department of Visual Sciences, University of Alabama at Birmingham, Birmingham, Alabama, USA. [3]Center for Mind/Brain Sciences, University of Trento, Rovereto, Italy. [4]These authors contributed equally to this work. Correspondence should be addressed to J.C.H. (hortonj@vision.ucsf.edu).

Received 27 June; accepted 12 September; published online 6 November 2011; doi:10.1038/nn.2958

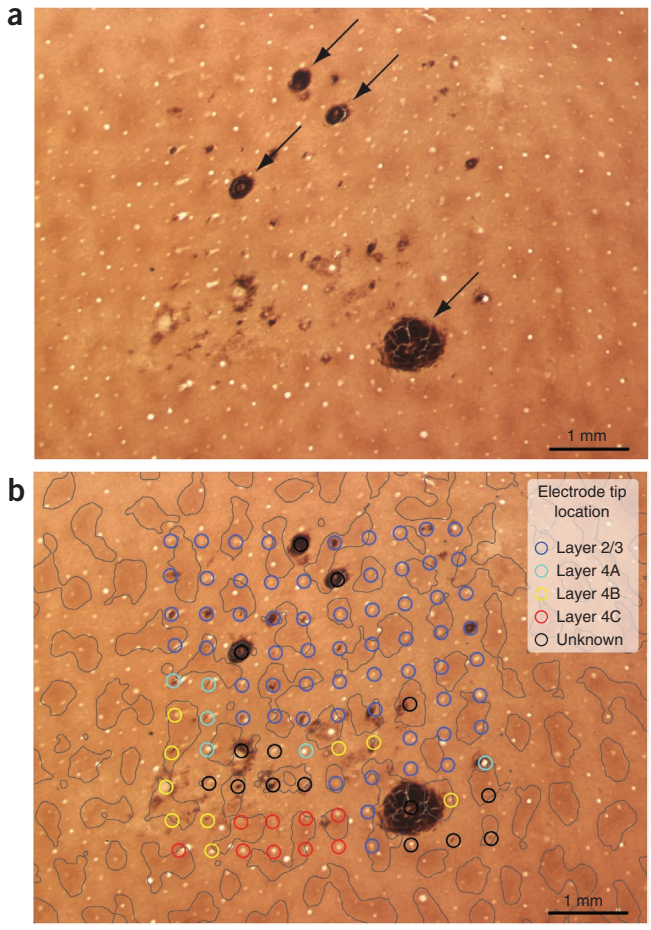


**Figure 1** Recovery of microelectrode penetrations. (**a**) Single tangential section 300 µm from the pial surface stained for cytochrome oxidase, revealing the electrode array footprint. Some of the electrodes caused bleeding in the tissue (arrows). (**b**) Same section, with a 75 µm radius circle centered on the hole left by each electrode. The circles are color-coded to indicate the layer where the electrode tip terminated. The contours outline the patches, defined by image processing as the darkest 33% of the tissue.

the electrode tips more deeply than intended into the cortex. In these cases, the resulting 10 × 10 grid was easy to identify because the holes were large, owing to the greater thickness of the electrodes at their base. Data from deep electrodes could not be used because our aim was to examine orientation tuning in layer 2/3 patches.

The boundaries of the patches were defined by thresholding cytochrome oxidase activity in the deepest section through layer 3. A circle of 75 µm radius, representing the maximum distance over which an electrode would be likely to detect action potentials from a cell, was centered on the hole left in the tissue by each electrode shaft[10]. At 42 of 61 sites in an example array (**Fig. 1b**), the circle was located entirely within the territory of a patch or interpatch in layer 2/3. In such cases, there was no doubt about the identity of cells recorded by the electrode. At 19 sites in this example, however, the circle crossed a patch/interpatch boundary. In this situation, the cells recorded by the electrode were designated as patch or interpatch on the basis of the location of the center of the circle. Usually the center pixel was relatively far from a patch boundary, so this approach classified most cells accurately. In a later analysis, we address the problem posed by electrodes that happened to straddle a patch boundary.

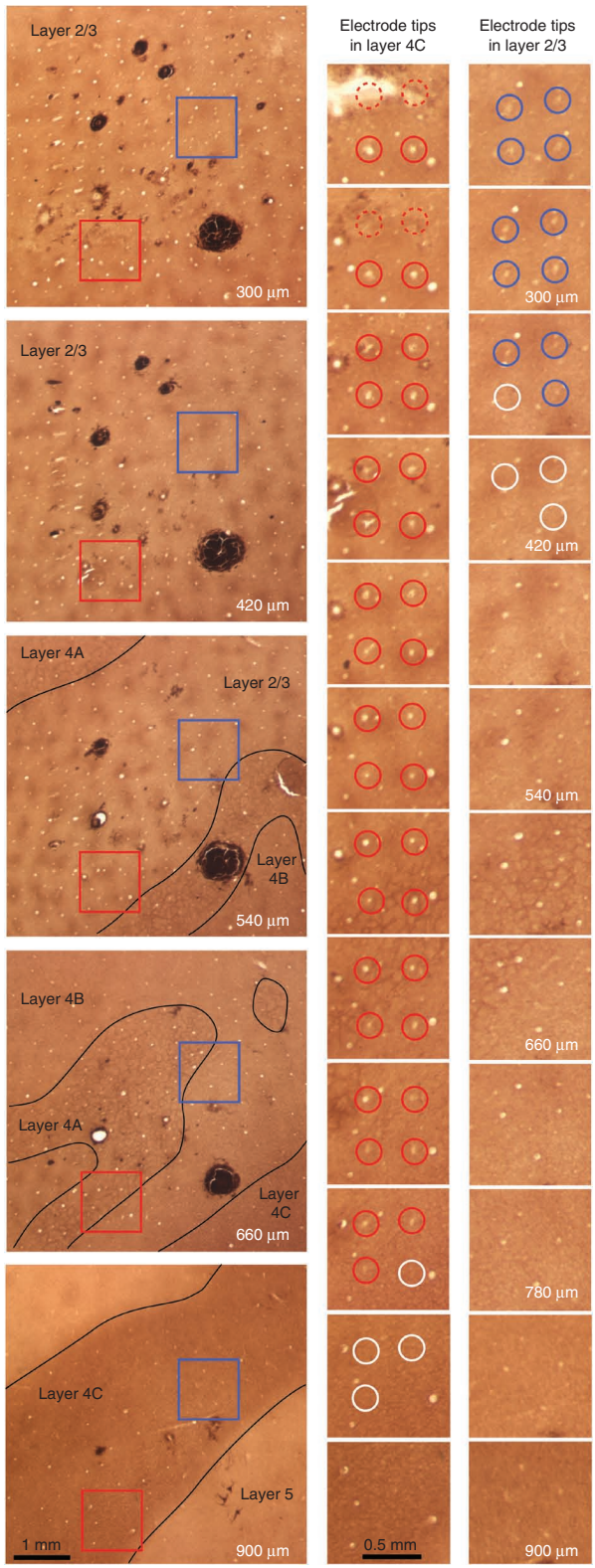


**Figure 2** Identification of electrode tip laminar locations. At left, five sections from the electrode implantation in **Figure 1** are shown at increasing cortical depth. Layers are defined by their characteristic pattern of cytochrome oxidase staining. At right, four electrodes ending in either layer 2/3 (blue box) or 4C (red box) are traced through serial 60-µm sections at higher magnification. The section where each electrode hole vanishes (white circles) is defined as the layer where the recording was made. Tissue damage in the most superficial section obscures electrode holes (dotted circles).

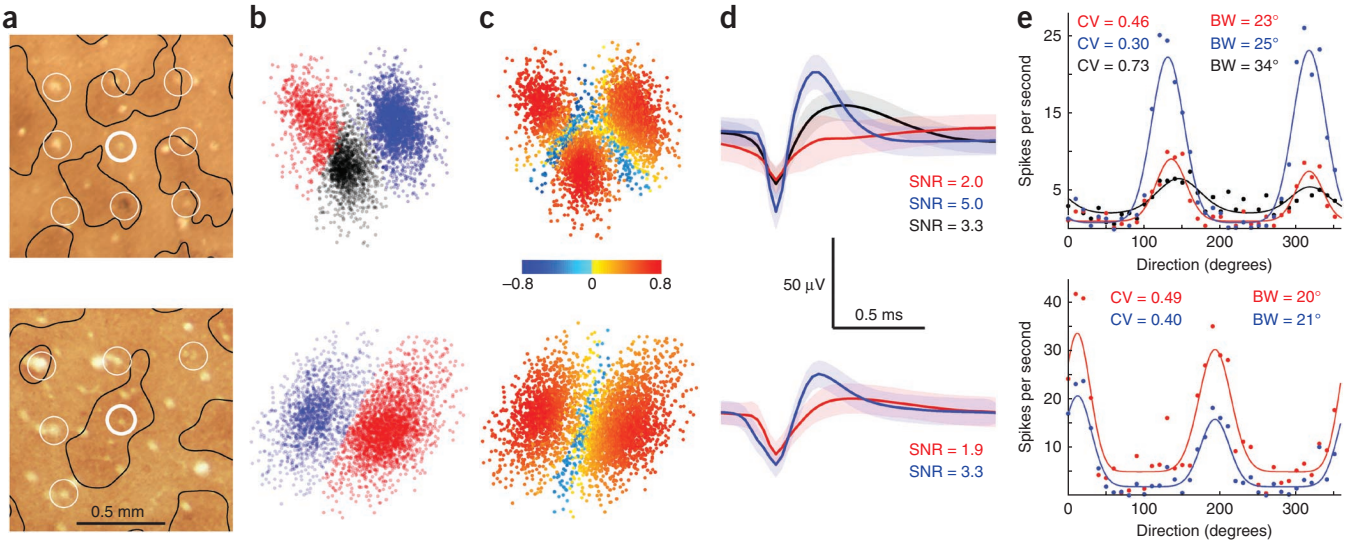


**Figure 3** Orientation tuning in an interpatch (top row) and patch (bottom row). (**a**) White circles mark electrode holes in a layer 2/3 cytochrome oxidase section, with sample recordings from the sites inside the bold circles. (**b**) *k*-means cluster analysis of a scatter plot of the coefficients from the first three principal components of each waveform. (**c**) Silhouette values, denoting in blue the potentially misassigned points. (**d**) Average waveforms of each cluster, ± s.d. (pale color margins). (**e**) Orientation tuning data plus fits computed for each waveform, with circular variance (CV) and bandwidth (BW) color-coded. Optimal tuning at each site is similar, owing to the existence of orientation columns.



## Recordings from electrode arrays

Immediately after electrode insertion, neurons had low firing rates and their extracellular potentials were small in amplitude, presumably from the trauma of driving the array into the cortex. Gradually the quality of recordings improved[6]. The recovery of cortical function was monitored at regular intervals by plotting the receptive fields of cells sampled on different electrodes. Once responses appeared robust, we presented drifting achromatic sine wave gratings on a computer monitor. To assess orientation tuning, the gratings were displayed for 2-s epochs, randomly varying the orientation in 10° intervals. Data were obtained from eight successful array insertions in five monkeys. From these eight arrays, 596 distinct waveforms were recorded from 366 electrodes located in layer 2/3.

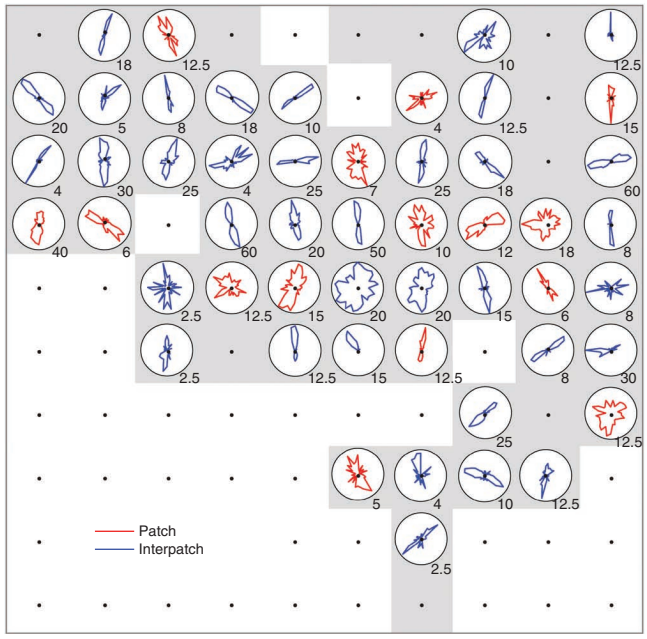


Recording electrodes landed by chance in patches or interpatches (**Fig. 3a**). On about half the electrodes, multiple distinct waveforms were observed. We performed *k*-means cluster analysis on the first three principal component coefficients (**Fig. 3b**). Because the clusters were not always perfectly segregated, it is possible that some waveforms were misassigned. To assess the error rate, we calculated a silhouette value, with negative values denoting a waveform potentially assigned to the wrong cluster (**Fig. 3c**)[11]. Less than 10% of the points in each cluster had a negative silhouette value. Average waveforms were derived from each cluster (**Fig. 3d**).

Firing rates as a function of the motion direction of the oriented grating were plotted for each distinct average waveform (**Fig. 3e**). When multiple waveforms were distinguished at a given electrode, they generally had a similar preferred orientation. However, they often varied considerably in the strength of orientation tuning. This property was defined using two different criteria: peak bandwidth and circular variance. Each measure provides useful information about a neuron's orientation selectivity[12]. Bandwidth reflects how sharply the cell's peak response is tuned and essentially ignores responses to other orientations. Circular variance takes into account the entire tuning curve, reflecting not only the shape of the peak but the firing rate at other orientations as well[13]. For these example recordings (**Fig. 3e**), circular variance ranged from 0.30 to 0.73 (where 0 is oriented and 1 is unoriented) and bandwidth ranged from 20° to 34°. To determine the impact of events potentially assigned to the wrong cluster, we recompiled the tuning curves in this example after eliminating all points with negative silhouette values. This precaution altered the values for circular variance

**Figure 4** Electrode array orientation tuning. Plots are from cells recorded from the array in **Figure 1**. Light gray shading indicates that the electrode tip was located in layer 2/3, either in a patch (red) or interpatch (blue). The polar axis corresponds to the direction of motion of an oriented grating and the radius indicates the mean response; the black number at lower right is the firing rate in spikes per second represented by the bounding circle. If multiple units were encountered, the waveform with the highest peak firing rate is shown for each electrode.

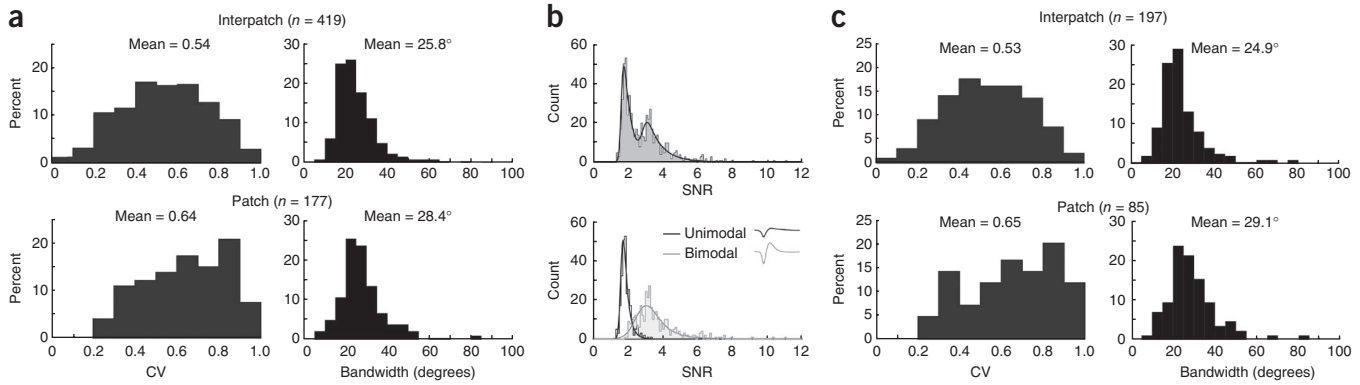


**Figure 5** Orientation selectivity of patches versus interpatches. (**a**) The distribution of circular variance (CV; 0 is oriented, 1 unoriented) and bandwidth (half-width at half-height of the larger peak). Both populations showed a wide range of orientation selectivity; on average, cells in patches were slightly less selective. (**b**) Top: histogram showing SNR for all waveforms, with a local minimum at 2.55. Bottom: histogram showing separate plots of SNR for waveforms with unimodal versus bimodal morphology. The intersection between the curves is close to 2.55. Waveforms with a unimodal shape had a lower SNR than those with a bimodal shape. Fits are exponentially modified Gaussians. (**c**) Orientation selectivity of bimodal waveforms with a SNR > 2.55. Elimination of low SNR and unimodal units did not change significantly the mean values for orientation selectivity: patches remained less orientation selective.



and bandwidth by less than 2%, suggesting that overlap of event clusters had only a modest effect on orientation tuning indices.

Orientation tuning curves were plotted for all the waveforms recorded by electrodes in layer 2/3. For the example array insertion (**Fig. 1**), 65 tips were located in layer 2/3. Cytochrome oxidase activity was obscured by local hemorrhage around 4 electrodes, so we excluded these sites from analysis. Only background noise was recorded at another 10 electrodes. Of the remaining 51 electrodes, 15 were situated in patches and 36 in interpatches. At first glance, the tuning curves show no striking difference between the orientation selectivity of neurons in patches versus interpatches (**Fig. 4**).

## Orientation tuning of patches versus interpatches

The population of neurons recorded in the upper layers showed a wide range in circular variance and bandwidth (**Supplementary Fig. 2**). For patch cells, the values for circular variance were mean 0.64 ± 0.19, median 0.66 ($n$ = 177) (**Fig. 5a**). For interpatch cells, the mean was 0.54 ± 0.20, median 0.54 ($n$ = 419). Overall, orientation tuning was weaker in patches than in interpatches ($P < 0.001$, Wilcoxon rank-sum test). This was true in three of five monkeys when analyzed individually ($P < 0.05$), with a nonsignificant trend in a fourth monkey. In one monkey, the circular variance was equal for patch and interpatch cells.

For patch cells, the bandwidth of orientation tuning curves had a mean of 28.4° ± 11.7° and a median of 26.8°. For interpatch cells, the values were mean 25.8° ± 10.9°, median 23.5° (**Fig. 5a**). The bandwidth difference between these two populations was 2.6° ($P < 0.001$, Wilcoxon rank-sum test). Neurons in patches had wider orientation bandwidths in four of five individual monkeys, although this trend reached significance ($P < 0.05$) in only one monkey.

In assessing orientation tuning, we presented drifting gratings at four different spatial frequencies: 0.5, 1, 2 and 4 cycles degree$^{-1}$. The spatial frequency that produced maximal firing at a cell's preferred orientation was used to calculate circular variance and bandwidth. Of note, there was no significant difference ($P > 0.98$, Wilcoxon rank-sum test) between the optimal spatial frequency for patch units (1.40 ± 0.68 cycles degree$^{-1}$) and interpatch units (1.42 ± 0.71 cycles degree$^{-1}$).

## Single-unit data

The electrode arrays yielded a mixture of multiple-unit and single-unit recordings. Multiple-unit activity might provide an inaccurate, low measure of orientation tuning strength by merging signals from an ensemble of well tuned cells that prefer different orientations. For this reason, we analyzed data gathered only from well isolated, single units.

For the 596 recorded waveforms, signal-to-noise ratio (SNR), defined as peak-to-trough amplitude divided by twice the s.d.[6], ranged from 1.3 to 11.0, with a mean of 2.89. The SNRs of recordings with 100-electrode arrays are usually lower than those from conventional microelectrodes[6]. The lower SNR is due to the fact that array electrodes have relatively low impedance (mean, 280 kΩ for the array in **Fig. 4**) and they cannot be advanced closer to cells to increase spike amplitude. Consequently, our data set included low-amplitude, multiple-unit recordings that would not have been collected had the recordings been done with mobile, high-impedance electrodes.

A histogram of the SNR for our recordings had a two-peaked distribution, with a local minimum at 2.55 (**Fig. 5b**). This trough corresponded closely to the intersection between the SNR distributions for average waveforms with a unimodal versus bimodal morphology (**Fig. 5b**). Unimodal average waveforms usually represent composite

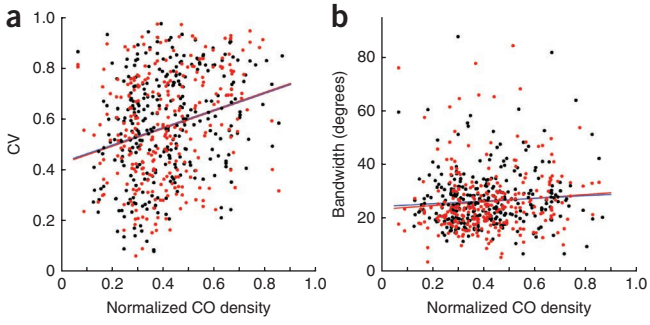


**Figure 6** Orientation selectivity versus cytochrome oxidase density. (**a**) Circular variance plotted against normalized cytochrome oxidase (CO) density confirms that cells with a higher circular variance (CV) are more likely to be present in darker CO regions (blue line, $R^2 = 0.067$). This correlation was significantly different from $R^2 = 0$ ($P < 0.01$, $t$-test). (**b**) Bandwidth plotted versus CO density showed no significant trend (blue line, $R^2 = 0.006$, $P = 0.052$, $t$-test). (**a**,**b**) When the subset of recordings with a bimodal waveform and SNR >2.55 were analyzed (encoded in red), both metrics showed weak correlations that were significantly different from $R^2 = 0$ (CV: $R^2 = 0.091$, $P < 0.01$; bandwidth: $R^2 = 0.015$, $P < 0.05$; both $t$-tests).

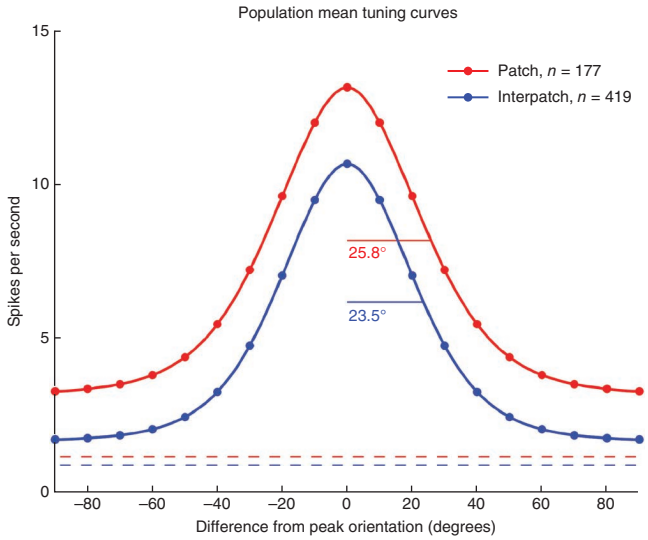


**Figure 7** Population mean tuning curves for patch versus interpatch neurons. Each unit's orientation data was fit with a function consisting of the sum of two Gaussians and an offset term. Shown here is the average of the Gaussian fits to the larger peak for all cells' tuning curves. There was a significant difference in the mean bandwidth ($P < 0.001$) and baseline firing rate ($P < 0.001$) for patch cells, although their response to visual stimulation had the same amplitude as for interpatch cells. The area under the patch curve was 49% greater, reflecting a higher overall firing rate. Dashed lines, mean spontaneous firing rates.

multiple-unit recordings, whereas bimodal waveforms are more likely to constitute single units[14–16].

We analyzed orientation selectivity for all waveforms that met two criteria: bimodal morphology and SNR >2.55 (**Fig. 5c**). This subset was considered separately because it was likely to consist predominately of single units. For patches ($n = 85$), the mean circular variance was 0.65 ± 0.21 (median 0.69). For interpatches ($n = 197$), the mean circular variance was 0.53 ± 0.20 (median 0.53). For patches, the mean bandwidth was 29.1° ± 12.1° (median 27.0°). For interpatches, it was 24.9° ± 11.6° (median 22.1°). For both measures of orientation selectivity, cells in patches were more broadly tuned than those in interpatches ($P < 0.001$, Wilcoxon rank-sum test). The elimination of low-SNR and unimodal waveforms made no appreciable difference in the mean or distribution of circular variance and orientation bandwidth. This implies that SNR and orientation selectivity are not related. Indeed, plots of waveform SNR versus circular variance and bandwidth showed no correlation (**Supplementary Fig. 3**).

### Cytochrome oxidase density and orientation selectivity

In histological sections processed for cytochrome oxidase activity, the darkest 33% of striate cortex is commonly designated as patches[17,18]. However, the exact percentage chosen to define patch boundaries is arbitrary. As mentioned earlier, the division of V1 into just two zones could misclassify cells recorded by electrodes located near the borders of patches. In addition, dichotomizing the cortex into two compartments might miss subtle trends in the spatial layout of oriented cells. For these reasons, we plotted circular variance and orientation bandwidth as continuous functions of cytochrome oxidase density (**Fig. 6**). Scatter plots confirmed that neurons with broader orientation tuning tended to be located in regions of darker cytochrome oxidase activity. The correlation was weak, and it remained weak even when considering just single units (bimodal and SNR >2.55). This analysis shows that changing the proportion of cortical territory assigned to patches does not alter the basic finding in this study.

### Mean population tuning curves

To compare the firing activity of cells recorded in patches ($n = 177$) to that in interpatches ($n = 419$), we averaged the Gaussian fits for the largest peak of each neuron's orientation tuning curve to generate mean tuning curves (**Fig. 7**). These showed a 2.3° greater bandwidth for patch cells.

At the peaks, the firing rate was greater for patch cells (patch mean, 13.2 ± 11.9 spikes per second; interpatch mean, 10.7 ± 10.6 spikes per second, $P < 0.01$, Wilcoxon rank-sum test). However, when the offsets were taken into account, the peak amplitude of the response to visual stimulation was similar (patch mean, 10.0 ± 9.6 spikes per second; interpatch mean, 9.0 ± 9.8 spikes per second, $P = 0.28$, Wilcoxon rank-sum test). The greater offset for patch cells was due to a stronger response to contours orthogonal to the optimal orientation (3.2 ± 4.2 spikes per second versus 1.7 ± 1.9 spikes per second, $P < 0.001$, Wilcoxon rank-sum test). The spontaneous activity, measured in the dark with no visual stimulation, was also slightly but significantly ($P < 0.002$, Wilcoxon rank-sum test) greater for patch cells (mean, 1.2 ± 1.8 spikes per second) than for interpatch cells (mean, 0.9 ± 1.6 spikes per second).

The area under each mean tuning curve represents the overall firing rate for each population of cells. The integrated area was 49% greater for patch cells than interpatch cells. This marked difference in physiological activity during visual stimulation may explain, in part, the stronger cytochrome oxidase activity present in patches.

These population mean tuning curves were compiled using the grating that yielded the maximum peak discharge rate (patch mean, 1.40 cycles degree$^{-1}$; interpatch mean, 1.42 cycles degree$^{-1}$). Even at the lowest spatial frequency tested (0.5 cycles degree$^{-1}$), the peak firing rate was significantly greater ($P < 0.01$) for patch cells (mean, 8.1 ± 9.6 spikes per second) than for interpatch cells (mean, 6.1 ± 7.0 spikes per second). It did not seem that at a spatial frequency lower than optimal, responses of interpatch cells were attenuated more than those of patch cells.

## DISCUSSION

The orientation tuning of cells was analyzed quantitatively by several investigators[19–22] following the original report that selectivity is sharply diminished in cytochrome oxidase patches of macaque striate cortex[4]. In these subsequent studies, no relationship was found between the degree of orientation tuning and the density of cytochrome oxidase staining in the upper layers. However, these investigators examined different primate species or did not cut histological sections parallel to the pial surface to reveal the two-dimensional layout of cytochrome oxidase patches. It is difficult to delineate patches in sections cut perpendicularly or obliquely to the cortical surface, and even more difficult to achieve reliable alignment with fragments of electrode tracks marked by occasional lesions in serial sections. For these reasons, the orientation tuning of patch cells in macaque striate cortex has remained an unresolved issue, even though these curious structures were discovered more than a quarter century ago[2,3].

The 100-electrode arrays were designed for chronic implantation in alert animals[9]. No previous study has to our knowledge described the appearance of the array footprint post-mortem in cortical tissue. A major advantage of the arrays for acute physiological studies is that for each electrode one can identify reliably the layer in which it terminates and establish precisely the correlation with cytochrome oxidase patches. Our data confirmed that patch cells were more broadly tuned for orientation than interpatch cells. However, the difference between the populations was exceedingly subtle; most cells in patches retained strong orientation selectivity (**Fig. 7**).

We harbored some doubts about the health of the cortex during our recordings because transient depression of neural activity occurred after each array implantation and intracortical hemorrhage was usually present post-mortem (**Fig. 1**). Tissue damage is less critical when arrays are used for chronic recordings because the cortex has more time to recover from the insult of electrode insertion. Several factors, however, suggested that the discrepancy between our findings and those reported originally[4] was not simply an artifact of using electrode arrays rather than single microelectrodes. First, the values for circular variance and orientation bandwidth we obtained closely resembled published data obtained from V1 using single microelectrodes (**Supplementary Fig. 2**)[12,19,23]. Second, one would expect injury from array insertion to degrade receptive field properties and reduce orientation selectivity, not increase it. Third, although multiple units were recorded on many electrodes, such recordings could not generate well tuned orientation curves if patch cells truly do lack orientation selectivity. Fourth, although it is true that cell isolation is generally inferior with electrode arrays compared with single microelectrodes, our findings held even after culling unimodal and low-SNR units (**Fig. 5c**). This result is consistent with a report that the orientation tuning of multiple-unit and single-unit activity recorded from V1 with 100-electrode arrays is highly correlated[24].

Orientation columns in macaque striate cortex converge in regions known as singularities or pinwheels[25,26]. Neuronal selectivity for orientation varies systematically according to local map structure. With 100-electrode arrays, it has been shown that cells near singularities are more broadly tuned for orientation than cells located in radiating iso-orientation domains[8]. If cytochrome oxidase patches coincide with singularities, this could explain the modest reduction in orientation selectivity displayed by patch cells (**Fig. 5**). Unfortunately, the spatial relationship between pinwheels and patches has been hard to establish because it is difficult to achieve secure alignment between intrinsic signal orientation maps and cytochrome oxidase histology, or even to define the exact location of pinwheel centers[27–31]. Optical imaging has not revealed any other zones in striate cortex that might harbor clusters of more poorly oriented cells[4].

Cells in patches send an exclusive projection to thin cytochrome oxidase stripes in V2. Dual retrograde tracer injections into adjacent thin and pale stripes have confirmed that projections from patches and interpatches to V2 are isolated strictly from each other[32,33]. This anatomy hints powerfully that patches have a specialized function, distinct from interpatches. Given that patches receive a direct projection from blue-yellow koniocellular geniculate neurons, it is natural to postulate that they are dedicated to color processing. Single-cell physiology and optical imaging have provided support for this idea[34–37]. However, the fact that a structure receives direct input from a class of color-encoding cells does not mean that it constitutes a separate color system. Layer 4Cβ, for example, receives direct input from red-green parvocellular neurons, but it is not considered a structure devoted to color rather than to form. A small population of unoriented cells is likely to exist in patches, fed by direct koniocellular input. These units may contribute to the slightly broader mean orientation tuning of patches. However, most cells in patches are well tuned, presumably because their strongest source of input arises from intracortical projections that build orientation selectivity[38].

It was previously thought that V1 color cells have radially symmetric, unoriented receptive fields[4]. Patches were expected to contain unoriented cells because they mediate color perception rather than edge detection. Subsequently, it has been learned that many neurons in V1 respond to both equiluminant color and luminance modulation, and that these color-luminance units are well oriented, with a mean circular variance of 0.40 (ref. 39). Many studies have confirmed that color-responsive cells in V1 can be orientation selective[22,40,41]. Even double-opponent cells, reportedly prevalent in patches[4], are tuned for orientation[42]. These observations suggest that there is no contradiction between the finding that patches retain orientation tuning and the idea that they are involved in color vision.

Several recent functional magnetic resonance imaging studies have shown that blood oxygen level–dependent signals in striate cortex can discriminate between stimuli that differ in color and orientation, indicating that orientation-selective chromatic mechanisms emerge early in the human visual system[43–45]. In one paradigm, subjects viewed gratings that alternated between red and green or between +45° and −45° (ref. 46). In the double-conjunction condition, the stimulus alternated simultaneously in color and orientation. The voxels that were most informative for the double-conjunction condition were distinct from those that were most informative for switches in color and orientation alone. This result implies that V1 contains local groups of cells jointly sensitive to orientation and color, perhaps corresponding to cytochrome oxidase patches.

Our recordings indicated that neurons in patches had a higher mean peak firing rate (13.2 spikes per second versus 10.7 spikes per second) in response to visual stimulation (**Fig. 7**). In addition, the response to the anti-preferred orientation was nearly twice as great (3.2 spikes per second versus 1.7 spikes per second). This difference in the offset of the tuning curves of patch cells contributed to their higher circular variance, but it did not account entirely for their broader tuning, because their peak orientation bandwidths averaged 10% wider (28.4° versus 25.8°). It would be interesting to compare surround inhibition for cells in patches versus interpatches, to see if this property contributes to the offset in firing rates.

A previous report noted that spike rates recorded in patches are 33% greater than in interpatches, but the result did not reach statistical significance because few neurons were sampled[47]. Our 100-electrode array recordings showed that patch cells had a 49% higher mean overall firing rate than interpatch cells. Metabolic demand from this enhanced neuronal activity probably explains in part the greater cytochrome oxidase content of patches compared with surrounding tissue. It also explains a curious finding from early 2-deoxyglucose studies. Under a wide variety of stimulus conditions, 2-deoxglucose uptake is greatest in patches[2,48,49]. This observation led directly to the idea that patches contain unoriented cells. It was hypothesized that they are more active metabolically because they respond equally to contours of all orientation[4]. It now seems that most patch cells are well oriented but simply have a higher intrinsic mean firing rate than interpatch cells, both under spontaneous conditions and when driven by visual activity.

## METHODS

Methods and any associated references are available in the online version of the paper at http://www.nature.com/natureneuroscience/.

*Note: Supplementary information is available on the Nature Neuroscience website.*

### ACKNOWLEDGMENTS

This work was supported by grants EY10217, EY10217-16A1S1 (J.C.H.), EY13676 (L.C.S.) and EY02162 (Beckman Vision Center) from the US National Eye Institute and by Research to Prevent Blindness. The California Regional Primate Research Center is supported by US National Institutes of Health Base Grant RR00169. C.M. Jocson provided technical assistance and M.K. Feusner assisted with computer programming.

### AUTHOR CONTRIBUTIONS

All authors participated in the physiological recording experiments, data analysis, and preparation of this paper.

**COMPETING FINANCIAL INTERESTS**
The authors declare no competing financial interests.

Published online at http://www.nature.com/natureneuroscience/.
Reprints and permissions information is available online at http://www.nature.com/reprints/index.html.

1. Heywood, C.A. & Kentridge, R.W. Achromatopsia, color vision, and cortex. *Neurol. Clin.* **21**, 483–500 (2003).
2. Horton, J.C. & Hubel, D.H. Regular patchy distribution of cytochrome oxidase staining in primary visual cortex of macaque monkey. *Nature* **292**, 762–764 (1981).
3. Wong-Riley, M. & Carroll, E.W. Effect of impulse blockage on cytochrome oxidase activity in monkey visual system. *Nature* **307**, 262–264 (1984).
4. Livingstone, M.S. & Hubel, D.H. Anatomy and physiology of a color system in the primate visual cortex. *J. Neurosci.* **4**, 309–356 (1984).
5. Martin, K.A.C. From enzymes to perception: a bridge too far? *Trends Neurosci.* **11**, 380–387 (1988).
6. Kelly, R.C. *et al.* Comparison of recordings from microelectrode arrays and single electrodes in the visual cortex. *J. Neurosci.* **27**, 261–264 (2007).
7. Smith, M.A. & Kohn, A. Spatial and temporal scales of neuronal correlation in primary visual cortex. *J. Neurosci.* **28**, 12591–12603 (2008).
8. Nauhaus, I., Benucci, A., Carandini, M. & Ringach, D.L. Neuronal selectivity and local map structure in visual cortex. *Neuron* **57**, 673–679 (2008).
9. Nordhausen, C.T., Maynard, E.M. & Normann, R.A. Single unit recording capabilities of a 100 microelectrode array. *Brain Res.* **726**, 129–140 (1996).
10. Henze, D.A. *et al.* Intracellular features predicted by extracellular recordings in the hippocampus in vivo. *J. Neurophysiol.* **84**, 390–400 (2000).
11. Kaufman, L. & Rousseeuw, P.J. *Finding Groups In Data: An Introduction to Cluster Analysis* (Wiley & Sons, New York, 1990).
12. Ringach, D.L., Shapley, R.M. & Hawken, M.J. Orientation selectivity in macaque V1: diversity and laminar dependence. *J. Neurosci.* **22**, 5639–5651 (2002).
13. Swindale, N.V. Orientation tuning curves: empirical description and estimation of parameters. *Biol. Cybern.* **78**, 45–56 (1998).
14. Eliades, S.J. & Wang, X. Chronic multi-electrode neural recording in free-roaming monkeys. *J. Neurosci. Methods* **172**, 201–214 (2008).
15. Nordhausen, C.T., Rousche, P.J. & Normann, R.A. Optimizing recording capabilities of the Utah Intracortical Electrode Array. *Brain Res.* **637**, 27–36 (1994).
16. Kim, S.J., Manyam, S.C., Warren, D.J. & Normann, R.A. Electrophysiological mapping of cat primary auditory cortex with multielectrode arrays. *Ann. Biomed. Eng.* **34**, 300–309 (2006).
17. Purves, D. & LaMantia, A. Development of blobs in the visual cortex of macaques. *J. Comp. Neurol.* **334**, 169–175 (1993).
18. Farias, M.F., Gattass, R., Piñón, M.C. & Ungerleider, L.G. Tangential distribution of cytochrome oxidase-rich blobs in the primary visual cortex of macaque monkeys. *J. Comp. Neurol.* **386**, 217–228 (1997).
19. Leventhal, A.G., Thompson, K.G., Liu, D., Zhou, Y. & Ault, S.J. Concomitant sensitivity to orientation, direction, and color of cells in layers 2, 3 and 4 of monkey striate cortex. *J. Neurosci.* **15**, 1808–1818 (1995).
20. Lennie, P., Krauskopf, J. & Sclar, G. Chromatic mechanisms in striate cortex of macaque. *J. Neurosci.* **10**, 649–669 (1990).
21. O'Keefe, L.P., Levitt, J.B., Kiper, D.C., Shapley, R.M. & Movshon, J.A. Functional organization of owl monkey lateral geniculate nucleus and visual cortex. *J. Neurophysiol.* **80**, 594–609 (1998).
22. Friedman, H.S., Zhou, H. & von der Heydt, R. The coding of uniform colour figures in monkey visual cortex. *J. Physiol. (Lond.)* **548**, 593–613 (2003).
23. Schiller, P.H., Finlay, B.L. & Volman, S.F. Quantitative studies of single-cell properties in monkey striate cortex. II. Orientation specificity and ocular dominance. *J. Neurophysiol.* **39**, 1320–1333 (1976).
24. Nauhaus, I. & Ringach, D.L. Precise alignment of micromachined electrode arrays with V1 functional maps. *J. Neurophysiol.* **97**, 3781–3789 (2007).
25. Blasdel, G.G. & Salama, G. Voltage-sensitive dyes reveal a modular organization in monkey striate cortex. *Nature* **321**, 579–585 (1986).
26. Bonhoeffer, T. & Grinvald, A. Iso-orientation domains in cat visual cortex are arranged in pinwheel-like patterns. *Nature* **353**, 429–431 (1991).
27. Polimeni, J.R., Granquist-Fraser, D., Wood, R.J. & Schwartz, E.L. Physical limits to spatial resolution of optical recording: clarifying the spatial structure of cortical hypercolumns. *Proc. Natl. Acad. Sci. USA* **102**, 4158–4163 (2005).
28. Blasdel, G.G. Orientation selectivity, preference, and continuity in monkey striate cortex. *J. Neurosci.* **12**, 3139–3161 (1992).
29. Bartfeld, E. & Grinvald, A. Relationships between orientation-preference pinwheels, cytochrome oxidase blobs, and ocular-dominance columns in primate striate cortex. *Proc. Natl. Acad. Sci. USA* **89**, 11905–11909 (1992).
30. Landisman, C.E. & Ts'o, D.Y. Color processing in macaque striate cortex: electrophysiological properties. *J. Neurophysiol.* **87**, 3138–3151 (2002).
31. Xu, X. *et al.* Functional organization of visual cortex in the owl monkey. *J. Neurosci.* **24**, 6237–6247 (2004).
32. Sincich, L.C. & Horton, J.C. Divided by cytochrome oxidase: a map of the projections from V1 to V2 in macaques. *Science* **295**, 1734–1737 (2002).
33. Sincich, L.C. & Horton, J.C. Input to V2 thin stripes arises from V1 cytochrome oxidase patches. *J. Neurosci.* **25**, 10087–10093 (2005).
34. Ts'o, D.Y. & Gilbert, C.D. The organization of chromatic and spatial interactions in the primate striate cortex. *J. Neurosci.* **8**, 1712–1727 (1988).
35. Landisman, C.E. & Ts'o, D.Y. Color processing in macaque striate cortex: relationships to ocular dominance, cytochrome oxidase, and orientation. *J. Neurophysiol.* **87**, 3126–3137 (2002).
36. Lu, H.D. & Roe, A.W. Functional organization of color domains in V1 and V2 of macaque monkey revealed by optical imaging. *Cereb. Cortex* **18**, 516–533 (2008).
37. Chatterjee, S. & Callaway, E.M. Parallel colour-opponent pathways to primary visual cortex. *Nature* **426**, 668–671 (2003).
38. Sincich, L.C. & Horton, J.C. The circuitry of V1 and V2: integration of color, form, and motion. *Annu. Rev. Neurosci.* **28**, 303–326 (2005).
39. Johnson, E.N., Hawken, M.J. & Shapley, R. The spatial transformation of color in the primary visual cortex of the macaque monkey. *Nat. Neurosci.* **4**, 409–416 (2001).
40. Yoshioka, T. & Dow, B.M. Color, orientation and cytochrome oxidase reactivity in areas V1, V2 and V4 of macaque monkey visual cortex. *Behav. Brain Res.* **76**, 71–88 (1996).
41. Horwitz, G.D., Chichilnisky, E.J. & Albright, T.D. Cone inputs to simple and complex cells in V1 of awake macaque. *J. Neurophysiol.* **97**, 3070–3081 (2007).
42. Johnson, E.N., Hawken, M.J. & Shapley, R. The orientation selectivity of color-responsive neurons in macaque V1. *J. Neurosci.* **28**, 8096–8106 (2008).
43. Sumner, P., Anderson, E.J., Sylvester, R., Haynes, J.D. & Rees, G. Combined orientation and colour information in human V1 for both L-M and S-cone chromatic axes. *Neuroimage* **39**, 814–824 (2008).
44. Engel, S.A. Adaptation of oriented and unoriented color-selective neurons in human visual areas. *Neuron* **45**, 613–623 (2005).
45. McDonald, J.S., Mannion, D.J., Goddard, E. & Clifford, C.W. Orientation-selective chromatic mechanisms in human visual cortex. *J. Vis.* **10**, 34 (2010).
46. Seymour, K., Clifford, C.W., Logothetis, N.K. & Bartels, A. Coding and binding of color and form in visual cortex. *Cereb. Cortex* **20**, 1946–1954 (2010).
47. DeYoe, E.A., Trusk, T.C. & Wong-Riley, M.T. Activity correlates of cytochrome oxidase-defined compartments in granular and supragranular layers of primary visual cortex of the macaque monkey. *Vis. Neurosci.* **12**, 629–639 (1995).
48. Kennedy, C., Des Rosiers, M.H. & Sakurada, O. Metabolic mapping of the primary visual system of the monkey by means of the autoradiographic $^{14}$[C] deoxyglucose technique. *Proc. Natl. Acad. Sci. USA* **73**, 4230–4234 (1976).
49. Tootell, R.B., Hamilton, S.L., Silverman, M.S. & Switkes, E. Functional anatomy of macaque striate cortex. I. Ocular dominance, binocular interactions, and baseline conditions. *J. Neurosci.* **8**, 1500–1530 (1988).

## ONLINE METHODS

**Recording procedures.** Experiments were conducted in eight adult macaques of both sexes, five rhesus (four male, one female) and three cynomolgus (all female), obtained from the California National Primate Research Center. All procedures were approved by the University of California, San Francisco Institutional Animal Care and Use Committee. Treatment with dexamethasone phosphate (2 mg per 24 h) was instituted 24 h before the experiment to reduce cerebral edema that might be induced by trauma from insertion of the electrode array. After administration of ketamine HCl (10 mg per kilogram body weight, intramuscularly), monkeys were ventilated with 1.0–1.5% isoflurane in a 1:1 mixture of $N_2O$ and $O_2$ to maintain general anesthesia. This alkyl halide is similar to halothane, the inhalation anesthetic used originally to investigate the orientation tuning of cells in cytochrome oxidase patches[4]. Electrocardiogram, respiratory rate, body temperature, blood oxygenation, end-tidal $CO_2$, urine output and inspired/expired concentrations of anesthetic gases were monitored continuously. Normal saline was given intravenously at a variable rate to maintain adequate urine output. After a cycloplegic agent was administered, the eyes were focused with contact lenses on a CRT monitor. Vecuronium bromide (60 $\mu g\ kg^{-1}\ h^{-1}$) was infused to prevent eye movements.

With the anesthetized monkey in a stereotaxic frame, an occipital craniotomy was performed over the opercular surface of V1. The dura was reflected to expose the cortex. A region relatively devoid of large surface vessels was selected for electrode array implantation. Despite this precaution, array insertion always produced some transient local bleeding (**Supplementary Fig. 1**). Electrodes were either 1.5 mm or 1.0 mm long, arranged in a 10 × 10 pattern, with each row 400 µm apart. The electrode tips were embedded in the cortex by striking the back of the array with a high-speed pneumatic piston. Our goal was to place the electrode tips into layer 2/3, where the cytochrome oxidase patches are most prominent. The array often sank too deeply into the cortex, lodging the electrode tips in layers 4–6. To achieve more superficial insertion, we positioned the piston so that the footplate, at the end of its travel, barely made contact with the back of the array. After chip insertion, local hemorrhage was removed by irrigation with artificial cerebrospinal fluid or cellulose swabs. The array was then covered with 1.5% agar to seal the craniotomy, eliminate pulsations and keep the cortex moist.

To position the stimulus screen at the correct location for each eye, the receptive fields of cells sampled by electrodes at the corners of the array were plotted. All recordings were made in opercular cortex, at eccentricities between 2° and 8°. For any given insertion, the aggregate receptive field subtended by the array electrodes depended on eccentricity, but it never exceeded 2°. After recordings were concluded at a given site, the agar was trimmed away and the chip was gently lifted from the cortex. A clean array was then implanted elsewhere. Implantations were made at one to three sites per hemisphere, depending on how rapidly the cortex recovered from array insertion. Recovery usually took 2–12 h at any given site; the array was relocated if cortical responsiveness remained depressed beyond 12 h.

At the end of the experiment, monkeys were killed with pentobarbital (150 mg $kg^{-1}$) and perfused with normal saline followed by 1 liter of 1% (wt/vol) paraformaldehyde in 0.1 M phosphate buffer, pH 7.4. The occipital lobes were flattened and sections were cut tangentially at 50–60 µm with a freezing microtome. Each section was dried on a slide and reacted for cytochrome oxidase.

A total of 33 array implantations were made in eight monkeys. In two monkeys, recordings were unsuccessful because of cerebral edema caused by insertion of the electrode array. In another, all the electrode tips ended below layer 2/3. In the remaining five, about half the array placements were unsatisfactory either because the array was implanted too deeply, cortical responsiveness never recovered after array insertion, or damage to the cortex from the array marred the cytochrome oxidase histology.

**Visual stimulation and data analysis.** A 17-inch monitor driven at 75 Hz was used to display achromatic sine wave gratings at 100% contrast, mean luminance 40 cd $m^{-2}$, through a circular aperture with a diameter of 8°. The gratings moved at 2° $s^{-1}$ for 2 s and were randomly interleaved at different orientations (every 10°) and spatial frequencies (0.5, 1.0, 2.0, 4.0 cycles $degree^{-1}$). These values for spatial frequency were appropriate for the eccentricity at which the recordings were made. Each stimulus was presented four to eight times, so a complete stimulus run took 20–40 min per eye. After testing one eye the screen was re-positioned and the other eye was stimulated. Over the course of several hours, about three stimulus runs were performed in each eye for each grid site.

Electrical potentials were recorded from 96 electrodes (4 electrodes on each array are left unconnected) and sampled at 30 kHz. The Cerebus data acquisition system (Blackrock Microsystems) extracted 1.5-ms segments containing spikes from the digitized signal, on the basis of a voltage threshold, and stored them for later analysis. The extracted spike shapes were sorted using principal component analysis and *k*-means clustering with Spike2 software (Cambridge Electronics Design). When multiple clusters were present, the validity of each waveform's assignment to its cluster was determined by calculating its silhouette value[11]. The silhouette value is a measure of how similar a given point is to other points in the same cluster versus other clusters. Using Matlab (Mathworks), silhouette values were calculated as

$$s(i) = [\min b(i,k) - a(i)] / \max[\min b(i,k), a(i)]$$

where $a(i)$ is the mean distance from point $i$ to the other points in its assigned cluster and $b(i,k)$ is the mean distance from point $i$ to the points in the nearest cluster $k$. The silhouette value ranges from −1 to +1. A negative value denotes a potentially misclassified waveform; $s(i)$ was negative for less than 10% of the points in the multiple clusters included in our data set.

Orientation tuning curves were compiled, plotting the mean firing rate during the 2-s stimulus period, without subtracting the spontaneous, background firing rate. For each tuning curve, data were plotted for the spatial frequency and eye that yielded the maximum firing rate at the cell's preferred orientation. The morphology of spikes sometimes changed from one stimulus run to the next. To make sure that no cell was inadvertently reanalyzed later as a different cell, a single, optimal stimulus run was used to compile the orientation tuning curves for all cells recorded by the electrode array. This was usually the last stimulus run performed at a given implantation site.

To calculate bandwidth, tuning data were smoothed with a Hanning window filter, with a half-width at half-height of 10°. They were then fit with a curve consisting of two Gaussian functions plus an offset term representing the firing rate at the nonpreferred orientations. The two Gaussians were allowed to fit the two largest peaks in the data without forcing them to be 180° apart. The orientation tuning bandwidth was defined as the half-width of the largest peak at half amplitude. Circular variance was calculated from the raw orientation tuning data as described previously[12]. Its value could range between 0 (perfect tuning at a single orientation) and 1 (no orientation preference).

**Cytochrome oxidase correlation with electrodes.** Digital photographs were taken of each cortical section using a SPOT RT color CCD camera (Diagnostic Instruments) mounted on an Olympus SZH10 microscope. The hole left by each electrode shaft was identified in the most superficial cortical section. The holes were 25–75 µm in diameter, which made it possible to confuse them with blood vessels. However, they could be identified reliably because they formed a regular lattice of perforations, with each electrode ~400 µm from the adjacent electrodes in the same row and column. In addition, many electrode holes were fringed by small clumps of extravasated erythrocytes. At higher magnification, blood vessels were clearly distinguished by the presence of an endothelium, which was absent in electrode holes. If doubt persisted, a hole could be followed through serial sections to see if it terminated at approximately the same cortical depth as adjacent electrodes.

It was possible to pinpoint the layer in which each electrode tip was located during the recording experiment by following each electrode hole from the pial surface through serial sections until it disappeared. The last 50 µm of each electrode is sharply tapered, reducing the size of the hole left in the cortex. We allowed for electrode tapering by assigning the tip to the section where the tissue defect left by the electrode completely disappeared. At the transition from layer 3 to 4A, the patches are replaced by a characteristic honeycomb pattern of cytochrome oxidase activity[50]. This obvious change in the pattern of cytochrome oxidase staining made it easy to identify those electrodes that penetrated beyond layer 3. Data analysis was confined to neurons recorded in layer 2/3, where patches have maximum contrast, to compare our results directly to those reported earlier[4].

To define the borders of patches, the cytochrome oxidase activity was analyzed in a single tangential histological section. We chose the deepest section through layer 3 that contained no layer 4A. Occasionally there were defects or blood clots in the section, ranging up to 1 mm in diameter, caused by damage from the electrode array. These blemishes were filled with the rubber stamp tool in Photoshop (Adobe Systems) by copying pixels from nearby, unaffected tissue. Microelectrode

recordings from these damaged regions were not included in our subsequent data analysis because the cytochrome oxidase compartment was unknown, but it was necessary to fill the defects to carry out the remaining image processing steps. White holes from large blood vessels and electrode shafts (>40 μm diameter) were filled in with pixels of the mean image grayscale value. The image was then imported into Matlab. An image erosion procedure was performed to eliminate bright or dark specks, such as small blood vessels, electrode holes or dust. A low-pass Fourier-filtered image was subtracted from the original image to correct for global shifts in cytochrome oxidase density due to fluctuation in cortical depth across the section. The resulting image was blurred with a 45-μm Gaussian filter. The darkest 33% of the pixels were designated as patches. To calculate the mean cytochrome oxidase density surrounding each electrode (**Fig. 6**), we normalized the images and then averaged the pixel values within a 50-μm radius.

50. Horton, J.C. Cytochrome oxidase patches: a new cytoarchitectonic feature of monkey visual cortex. *Phil. Trans. R. Soc. Lond. B* **304**, 199–253 (1984).




doi:10.1038/nn.2958